Subject-Specific Finite Element Model of the Pelvis: Development, Validation and Sensitivity Studies

Andrew E. Anderson
Department of Bioengineering,
University of Utah,
50 South Central Campus Drive,
Room 2480,
Salt Lake City, UT

Christopher L. Peters
Department of Orthopedics,
University of Utah Medical Center,
Salt Lake City, UT

Benjamin D. Tuttle
Department of Bioengineering,
University of Utah,
50 South Central Campus Drive,
Room 2480,
Salt Lake City, UT

Jeffrey A. Weiss[1]
Department of Bioengineering,
University of Utah,
50 South Central Campus Drive,
Room 2480,
Salt Lake City, UT and
Department of Orthopedics,
University of Utah Medical Center,
Salt Lake City, UT
e-mail: jeff.weiss@utah.edu

A better understanding of the three-dimensional mechanics of the pelvis, at the patient-specific level, may lead to improved treatment modalities. Although finite element (FE) models of the pelvis have been developed, validation by direct comparison with subject-specific strains has not been performed, and previous models used simplifying assumptions regarding geometry and material properties. The objectives of this study were to develop and validate a realistic FE model of the pelvis using subject-specific estimates of bone geometry, location-dependent cortical thickness and trabecular bone elastic modulus, and to assess the sensitivity of FE strain predictions to assumptions regarding cortical bone thickness as well as bone and cartilage material properties. A FE model of a cadaveric pelvis was created using subject-specific computed tomography image data. Acetabular loading was applied to the same pelvis using a prosthetic femoral stem in a fashion that could be easily duplicated in the computational model. Cortical bone strains were monitored with rosette strain gauges in ten locations on the left hemipelvis. FE strain predictions were compared directly with experimental results for validation. Overall, baseline FE predictions were strongly correlated with experimental results ($r^2 = 0.824$), with a best-fit line that was not statistically different than the line $y = x$ (experimental strains = FE predicted strains). Changes to cortical bone thickness and elastic modulus had the largest effect on cortical bone strains. The FE model was less sensitive to changes in all other parameters. The methods developed and validated in this study will be useful for creating and analyzing patient-specific FE models to better understand the biomechanics of the pelvis. [DOI: 10.1115/1.1894148]

Keywords: Pelvis, Finite Element, Biomechanics, Strain Gauges

Introduction

The acetabulum and adjoining pelvic bones are one of the most important weight bearing structures in the human body. Forces as high as 5.5 times body weight are transferred from the femur to the acetabulum during activities such as running and stair climbing [1–3]. The structure of the pelvis is a sandwich material, with the thin layers of cortical bone carrying most of the load. Despite its efficient structure, the pelvis can become damaged due to altered loading. Side impact forces, such as those generated in car accidents, are notorious for generating pelvic fractures. The fracture itself often causes multiple internal trauma leading to a mortality rate on the order of 12%–37% [4,5]. In addition to pelvic fractures, it has been hypothesized that subtle alterations in pelvic geometry (i.e., pelvic dysplasia) lead to osteoarthritis [6–11]. In fact, secondary causes of osteoarthritis, such as undiagnosed pelvic dysplasia, appear to be more prevalent among candidates for total hip arthroplasty (THA) than primary arthritis [10–13]. Michaeli et al. reported that nearly 76% of THA recipients exhibited signs of a dysplastic joint—a condition that went unrecognized prior to surgery [3]. Nevertheless, the relationship between pelvic dysplasia and osteoarthritis remains controversial since there is no direct quantitative evidence linking the two together.

Simplified mathematical models, experimental contact analyses, and force telemetry data have been used to estimate joint contact forces at the acetabulum [1–3,14–21]. These studies provide valuable information concerning overall joint mechanics but do not yield estimates of the surrounding bone stresses and strains. It would be wise to develop methods capable of quantifying the mechanics beyond the acetabular contact interface since there is evidence to suggest that the surrounding bone plays a pivotal role in the progression of diseases such as osteoarthritis [22–24]. A better understanding of the mechanics for the entire pelvis could lead to improved implant designs, surgical approaches, diagnosis, and may present the framework necessary for preoperative surgical planning. Specifically, an analysis of the stress distribution in and around the pelvic joint may clarify the mechanical relationship between pelvic geometry and predisposition to osteoarthritis.

It is difficult to assess the stress and strain distribution throughout the entire pelvis using simplified mathematical models, implanted prostheses, or via experiments with cadaveric tissue. An alternative approach to analyze pelvic mechanics is the finite element (FE) method, which can accommodate large intersubject variations in bone geometry and material properties. The potential benefit of patient-specific FE analysis becomes clear when one considers how difficult (if not impossible) it would be to assemble a population of donor tissue that exhibits a specific pathology such as pelvic dysplasia.

The objectives of this study were to develop and validate a FE model of the pelvis using subject-specific estimates of bone geometry, location-dependent cortical thickness and trabecular bone elastic modulus, and to assess the sensitivity of FE cortical strain predictions to cortical bone thickness and bone and cartilage material properties. The following hypotheses were tested: (1) A FE

[1]To whom correspondence should be addressed.

Contributed by the Bioengineering Division for publication In the JOURNAL OF BIOMECHANICAL ENGINEERING. Manuscript receieved January 12, 2004; revision received January 25, 2005, Associate Editor: Christopher Jacobs. Technical editor Frank Yin.

model of the pelvis that incorporated subject-specific geometry, cortical bone thickness, and position dependent trabecular bone elastic modulus would accurately predict cortical bone strains and (2) a subject-specific FE model of the pelvis would be more accurate than models that assume average cortical bone thickness and trabecular elastic modulus.

Materials and Methods

A combined experimental and computational protocol was used to develop and validate a subject-specific three-dimensional model of a 68 y/o female cadaveric pelvis (International Bioresearch Solutions, Tucson, AZ). The pelvic joint was visually screened for large-scale osteoarthritis prior to the study.

Experimental Study. The sacroiliac joint and all soft tissues, with the exception of articular cartilage, were removed. A registration block and wires were attached to the iliac crest. The block allowed for spatial registration of experimental and FE coordinate systems, while the wires served as a guide to reproduce the boundary conditions used in the experimental model [25]. A computed tomography (CT) scan (512×512 acquisition matrix, 225 mm field of view (FOV), in-plane resolution$=0.44\times0.44$ mm, slice thickness$=0.6$ mm, 354 slices) was obtained in a superior to inferior fashion using a Marconi MX8000 scanner (Philips Medical Systems, Bothell, WA). A bone mineral density (BMD) phantom (BMD-UHA, Kyoto Kagaku Co., Kyoto, Japan), consisting of 21 rectangular blocks of urethane with varying concentrations of hydroxyapaptite ($0-400$ mg/cm^3, 20 mg/cm^3 increments) was also scanned with the same field of view and energy settings. CT data from the BMD phantom were averaged over each block to obtain a relationship between CT scanner pixel intensity and calcium equivalent bone density.

The mounting and loading of the pelvis followed a protocol similar to that described by Dalstra et al. [26]. The iliac crests were submerged in a mounting pan of catalyzed polymer resin (Bondo, Mar-Hyde, Atlanta, GA) to the depth defined by the iliac guide wires. Ten three-element rectangular rosette strain gauges (WA-060WR-120, Vishay Measurements Group, Raleigh, NC), representing 30 channels of data, were attached to the left hemipelvis at locations around the acetabulum, pubis, ischium, and ilium. Vertically oriented loads of 0.25, 0.50, 0.75, and 1.0 X body weight (559 N) were applied to the acetabulum by displacing a femoral prosthesis, attached to a linear actuator (Fig. 1). The femoral implant was displaced continuously until the appropriate load was reached at which time the displacement was held constant, allowing stress relaxation, until the load relaxed to a value greater than 95% of the original with a load-time slope less than 0.25 N/s for at least 60 s. The average time to reach quasistatic equilibrium for each loading scenario was 6 min. An average of the rosette gauge readings $(\varepsilon_1,\varepsilon_2,\varepsilon_3)$ for the last ten seconds of the equilibrium period was obtained and then converted to in-plane principal strains $(\varepsilon_P,\varepsilon_Q)$ using the relationship [27]

$$\varepsilon_{P,Q}=\frac{\varepsilon_1+\varepsilon_3}{2}\pm\frac{1}{\sqrt{2}}\sqrt{(\varepsilon_1-\varepsilon_2)^2+(\varepsilon_2-\varepsilon_3)^2}. \quad (1)$$

Three-dimensional (3D) coordinates of the strain gauges and registration block were determined in a laboratory reference frame using an electromagnetic digitizer (Model BE-3DX, Immersion Corp., San Jose, CA). Geometric features of the pelvis were digitized to determine the accuracy of the geometry reconstruction.

Geometry Extraction and Mesh Generation. Contours for the outer cortex and the boundary of the cortical and trabecular bone, registration block, and guide wires were extracted from the CT data via manual segmentation (Fig. 2). Points comprising the contours were triangulated [28] to form a polygonal surface, which was then decimated [29] and smoothed [30] to form the final surface using VTK (Kitware Inc., Clifton Park, NY) [31] (Fig. 2). A volumetric tetrahedral mesh was created from the final surface

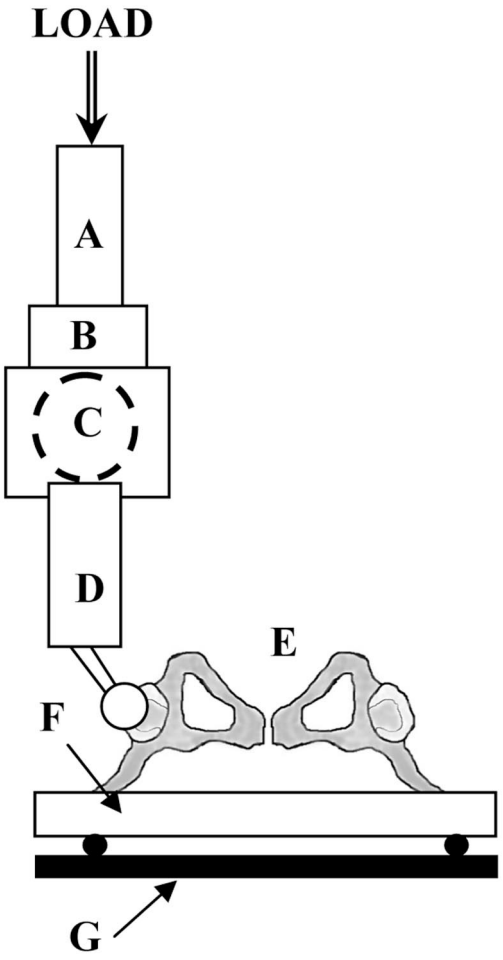

Fig. 1 Schematic of fixture for loading the pelvis via a femoral implant component. (*a*) actuator, (*b*) load cell, (*c*) ball joint, (*d*) femoral component, (*e*) pelvis, (*f*) mounting pan for embedding pelvis, and (*g*) lockable *X-Y* translation table.

to represent the outer cortex (CUBIT, Sandia National Laboratories, Albuquerque, NM). A four-node, 24 degree-of-freedom tetrahedral element was used to represent trabecular bone [32]. This element has three translational and rotational degrees of freedom at each node. Mesh refinement tests were performed with this

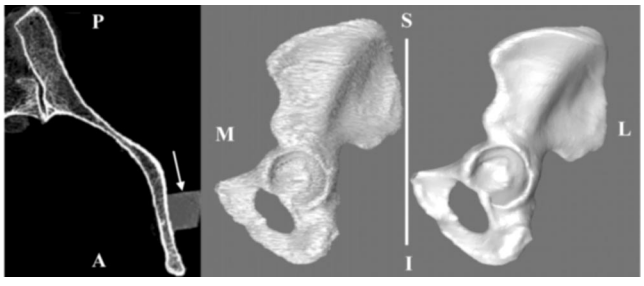

Fig. 2 Left—CT image slice at the level of the ilium, showing the registration block (arrow) and the distinct boundary between cortical and trabecular bone. Middle—the original polygonal surface representing the cortical bone was reconstructed by Delaunay triangulation of the points composing the segmented contours. Right—polygonal surface after decimation to reduce the number of polygons and smoothing to reduce high-frequency digitizing artifact. A—anterior, P—posterior, M—medial, L—lateral, I—inferior, S—superior.

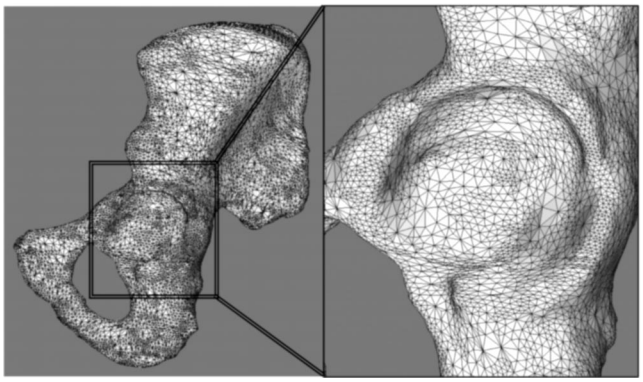

Fig. 3 Left—FE mesh of the pelvis, composed of 190,000 tetrahedral elements and 31,000 shell elements. Right—close-up view of the mesh at the acetabulum.

element using a model of a cantilever beam under a tip load with a thickness that was 10% of the beam length. FE-predicted tip deflections reached an asymptote of 4% error with respect to an analytical solution when at least three tetrahedral elements were used through the thickness of the beam.

Cortical bone was represented with quadratic three-node shell elements [33]. The elements were based on the Hughes-Liu shell [34,35], which has three translational and rotational degrees of freedom per node, with selective-reduced integration to suppress zero-energy modes [36]. The geometry of the shells was based on the nodes of the outside faces of the tetrahedral elements, on the outer surface of the pelvis. The shell reference surface and shell element normal were defined so that the cortical thickness pointed inward toward the interface between cortical and trabecular bone. This approach resulted in an overlap of one cortical bone thickness between the tetrahedral solid element and thin shell element. The elastic modulus for all tetrahedral element nodes in this region of overlap was set to 0 MPa. Mesh refinement tests showed that the three-node shell was nearly as accurate as using three tetrahedral elements through the thickness of the beam ($<5\%$ error with respect to analytical solution).

The density of the FE mesh was adjusted until it was at or above the beam mesh density required to achieve an error of 4%. The final surface mesh density was 0.5 shell elements/mm^2 with a volumetric density of 2.5 tetrahedral elements/mm^3. The final FE model consisted of 190,000 tetrahedral elements for trabecular bone and 31,000 shell elements for cortical bone (Fig. 3). Acetabular cartilage was represented with 350 triangular shell elements with a constant thickness of 2 mm, determined by averaging the distance between the implant and acetabulum in the neutral kinematic position.

Position-Dependent Cortical Thickness. An algorithm was developed to determine the thickness of the cortex based on the distances between the polygonal surfaces representing the outer cortex and the boundary between the cortical and trabecular bone. Vectors were constructed between each node on the cortical surface and the 100 nearest nodes on the surface defining the cortical-trabecular boundary. Cortical thickness was determined by minimizing both the distance between the nodes of the surfaces and the angle of the dot product between the surface normal of the cortical surface with that of each corresponding trabecular vector. In areas of high curvature (such as the acetabular rim), special consideration of thickness was necessary (Fig. 4). When the above-described algorithm reported a thickness value that exceeded 1.5 times the smallest distance between the nodes, the smallest distance between nodes on the two surfaces was used. The minimum value of nodal thickness was assumed to be 0.44 mm or the width of one pixel (FOV=225, FOV/512 =0.44 mm/pixel). The algorithm was tested using polygonal surfaces representing parallel planes, concentric spheres, and layered boxes with varying mesh densities.

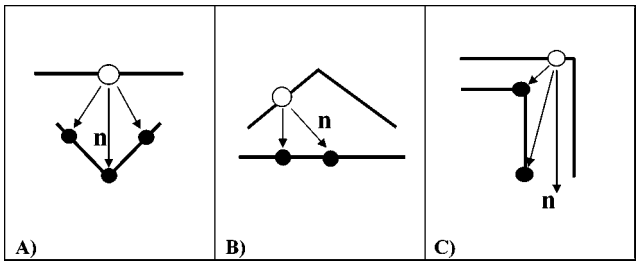

Fig. 4 Schematics illustrating the special cases considered in determination of cortical thickness. Both the distance between the surfaces and the angle of the dot product between the normal vector (n) with that of the vector created by subtracting the trabecular and cortical node coordinates were considered. Nodes on the cortical surface are represented as open circles, while nodes on the trabecular surface are shown as filled circles. Case A—the smallest angle of the dot product between the cortical node and nearest trabecular node neighbor yields the desired thickness measurement. Case B—the smallest distance between nodes provides the desired thickness measurement. Case C—the normal vector (n) from the cortical node does not intersect the trabecular surface. For cases B and C, a weighting scheme was applied such that the smallest distance between the nodes was taken as the cortical thickness when the originally reported thickness value exceeded 1.5 X the smallest distance between nodes on the two surfaces.

Assessment of Cortical Bone Thickness. A custom-built phantom was used to assess the accuracy of cortical thickness measurements (Fig 5) [37]. Ten aluminum tubes (wall thickness 0.127–2.921 mm) were fit into a 70 mm dia. Lucite disc. The centers of the aluminum tubes were filled with Lucite rods so that both the inner and outer surfaces of the tubes were surrounded by a soft tissue equivalent material [38,39]. Aluminum has an x-ray attenuation coefficient that is similar to cortical bone [37]. The phantom was scanned with the same CT scanner field of view and energy settings used for the cadaveric pelvis and bone mineral density phantom. The *z* axis of the scanner was aligned flush with the top edge of the tissue phantom to prevent volume averaging between successive slices. The inner and outer circumferences of the tubes were segmented from the CT image data using the same

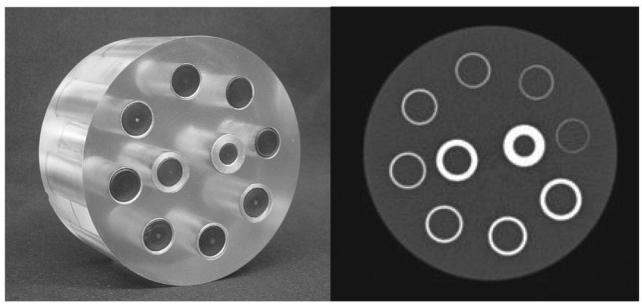

Fig. 5 Left—tissue equivalent phantom containing 10 aluminum tubes used to simulate cortical bone with varying thickness. The phantom was scanned with a CT scanner and manually segmented to determine the accuracy of cortical bone reconstruction. Right—cross-sectional CT image of the cortical bone phantom. Changes in thickness can be seen for the thicker tubes but become less apparent as the tube wall thickness decreases.

Table 1 Models studied for FE sensitivity analysis. Deviations in material properties and cortical thickness were taken from experimentally measured/estimated values (EXP) as well as data reported in the literature.

Type	Models analyzed	Reference
CST	Thickness = ±0, 0.5, 1 SD (0.49 mm)	EXP
CTEM	E = 45, 164, 456 MPa (quartiles)	EXP
CST/CTEM	Thickness = 1.41 mm, E = 164 MPa	EXP
SSCV	ν = 0.2, ν = 0.39	[57]
SSTV	ν = 0.29	[55]
SSCM	E = ±1 SD (1.62 GPa)	[58]
ACT	Thickness = 0.0, 4.0 mm (Min/Max)	EXP
ACEM	E = 1.36, 7.79 MPa (Min/Max)	[59]
OVERLAP	Surface tet. nodes = Max trabecular modulus	NA

technique to extract the pelvic geometry. The surfaces were meshed and the thickness algorithm was used to determine wall thickness.

Material Properties and Boundary Conditions. The femoral implant was represented as rigid while cortical and trabecular bone were represented as isotropic hypoelastic. Baseline material properties for cortical bone were E = 17 GPa and Poisson's ratio (ν) = 0.3 [26]. A linear relationship was established between CT scanner pixel intensity and calcium equivalent density using the CT image data from the BMD solid phantom

$$\rho_{ca} = 0.0008 \times \mathrm{INT} - 0.8037 \quad (r^2 = 0.9938). \tag{2}$$

Here ρ_{ca} is the calcium equivalent density of trabecular bone (g/cm^3) and INT is the CT scanner intensity value (0–4095). Next, a relationship was used to convert calcium equivalent density (ρ_{ca}) to apparent bone density (ρ_{app}) [40]

$$\rho_{app} = \frac{\rho_{ca}}{0.626}. \tag{3}$$

Finally, an empirical relationship was used to convert apparent density of pelvic trabecular bone to elastic modulus for each node [40]

$$E = 2017.3(\rho_{app})^{2.46}, \tag{4}$$

where E is the elastic modulus (MPa) and ρ_{app} is the apparent density of the trabecular bone (g/cm^3). Nodal moduli were averaged to assign an element modulus. Acetabular articular cartilage was represented as a hyperelastic Mooney-Rivlin material [41]. Coefficients C_1 and C_2 were selected as 4.1 MPa and 0.41 MPa, respectively, with Poisson's ratio = 0.4 [42].

A FE coordinate system was created from the polygonal surface of the reconstructed registration block. A corresponding coordinate system was established for the experimental measurements using the digitized coordinates of the registration block [25]. To establish the neutral kinematic position, a transformation was applied to the FE model to align it with the experimental coordinate system. Nodes superior to the iliac guide wires and nodes along the pubis synthesis joint were constrained to simulate the experiment. Contact was enforced between the femoral implant and cartilage while load was applied to the implant using the same magnitude and direction measured experimentally. Analyses were performed with the implicit time integration capabilities of LS-DYNA (Livermore Software Technology Corporation, Livermore, CA) on a Compaq Alphaserver DS20E (2 667 MHz processors). Each model required approximately 3 h of wall clock time and 1.1 GB of memory.

Sensitivity Studies. Sensitivity studies were performed to assess the effects of variations in assumed and estimated material properties and cortical thickness on predicted cortical surface strains. The assumed parameters were cortical bone Poisson's ratio, trabecular bone Poisson's ratio, cartilage elastic modulus, and cortical bone elastic modulus. The estimated parameters were trabecular elastic modulus and cortical bone thickness. Variations in assumed parameters were based on standard deviations from the literature (Table 1). The trabecular elastic modulus and cortical thickness were varied to reflect the median and interquartile range estimated computationally. The FE models included constant cortical shell thickness (CST), constant trabecular elastic modulus (CTEM), constant shell thickness and elastic modulus (CST/CTEM), and subject-specific models (position dependent trabecular elastic modulus and cortical thickness), with alterations in cortical bone Poisson's ratio, trabecular bone Poisson's ratio, cortical elastic modulus, articular cartilage thickness, and articular cartilage elastic modulus. A sensitivity model (OVERLAP) was analyzed to determine the cortical surface strain effects due to overlap between the cortical shell and tetrahedral elements. For the overlap model the tetrahedral surface nodes were assigned the maximum elastic modulus estimated from the cadaveric CT image data (3829 MPa). The surface nodes were averaged to estimate the elastic modulus for the each tetrahedral element as was done in the subject-specific model. The sensitivity of each model, S, was defined as

$$S = \frac{\%\ \text{change in slope}}{\%\ \text{change in input parameter}}. \tag{5}$$

The numerator in Eq. (5) is the percent change in slope of the best-fit lines between the sensitivity model and baseline subject-specific model. The denominator is the percent change in the model input parameter between the sensitivity model and the baseline subject-specific model. For those sensitivity models that investigated constant inputs such as cortical thickness and trabecular bone elastic modulus, the change in constant model input parameters was used in the denominator.

Data Analysis. FE predictions of cortical principal strains were averaged over elements that were located beneath each strain gauge. A rectangular perimeter, representing each strain gauge, was created on the surface of the FE mesh using digitized points from the experiment. Strains for a shell were included in the average if at least 50% of its area was within the perimeter. FE predicted strains were plotted against experimental strains. Best-fit lines and r^2 values were reported for each model at all loads. Statistical tests (α = 0.05) were performed to compare the slope and y intercept of the subject-specific best-fit line with the line $y = x$ (experimental strains = FE Strains) to test the null hypothesis: There was no significant difference between FE predicted strains and experimental strains [43]. Statistical tests were used to test differences between the slope of the best-fit line, and r^2 values for each sensitivity model with the baseline subject-specific model [43].

Results

Reconstruction of Pelvic Geometry. The geometry reconstruction techniques yielded a faithful reproduction of the measured geometric features of the pelvis (Fig. 6). Correlation be-

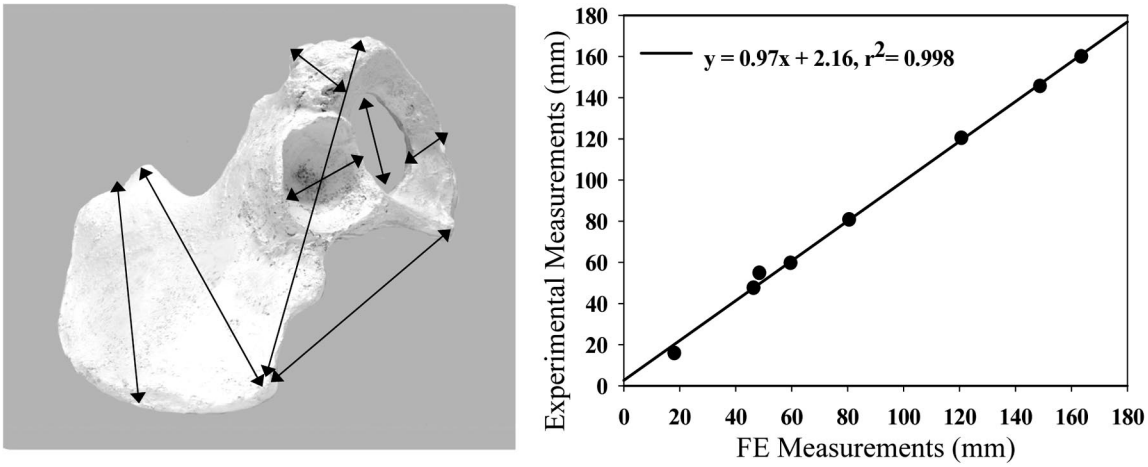

Fig. 6 Left—schematic showing the length measurements that were obtained from the cadaveric pelvis with an electromagnetic digitizer. Measurements were based on identifiable anatomical features of the iliac wing, ischium, obturator foramen, pubis, and acetabulum. Right—excellent agreement was observed between experimental measurements and the FE mesh dimensions, yielding a total error of less than 3%.

tween measurements on the cadaveric pelvis with the corresponding FE mesh was strong ($r^2=0.998$). There was no statistical difference between the slope and y intercept of the regression line and the line $y=x$.

Cortical Bone Thickness. The thickness algorithm accurately predicted thickness using simple polygonal surfaces with known distances between the surfaces. For parallel planes and concentric spheres, errors were ±0.004%. For the layered boxes, the rms error was ±2%. For all surfaces, errors decreased with increasing surface resolution. The above errors are based on polygonal surfaces with a resolution similar to the pelvis FE mesh.

The thickness algorithm estimated aluminum tube wall thickness accurately (less than ±10% error) for tubes with thicknesses between 0.762 and 2.9210 mm (Table 2). The reported standard deviation in nodal thickness for these tubes was also less than 10% of the average nodal thickness (Table 2). Therefore individual nodal thickness values did not deviate much from the average nodal thickness. However, errors in thickness increased progressively for tubes with wall thickness between 0.127 and 0.635 mm.

Cortical bone thickness ranged from 0.44–4.00 mm [mean 1.41±0.49 mm (SD)] (Fig. 7). Cortical thickness was highest along the iliac crest, the ascending pubis ramus, at the gluteal surface, and around the acetabular rim. Cortical bone was thin at the acetabular cup, the ischial tuberosity, the iliac fossa and the area surrounding the pubic tubercle.

Trabecular Bone Elastic Modulus. Trabecular elastic modulus ranged from 2.5–3829.0 MPa (mean=338 MPa, median =164 MPa, interquartile range=45–456 MPa). Data were significantly skewed to the right (positively skewed) so the median and bounds of the interquartile range were used for sensitivity models rather than the arithmetic mean and standard deviation. Areas of high modulus were predominately near muscle insertion sites and within the subchondral bone surrounding the acetabulum. Areas of low modulus were located near the sacroiliac joint, pubis joint, and along the ischial tuberosity and the interior of the ilium.

FE Model Predictions. FE predicted von Mises stresses for the subject-specific model ranged from 0–44 MPa and were greatest near the pubis-symphasis joint, superior acetabular rim, and on the ilium just superior to the acetabulum for each load applied (Fig. 8). Baseline FE predictions of principal strains showed strong correlation ($r^2=0.824$) with experimental measurements (Fig. 9, top panel) and had a best-fit line that was not statistically different than $y=x$ (experimental strains=FE Strains), (Table 3).

Coefficients of determination and y-intercept values were not statistically different than the subject-specific model for all sensitivity models analyzed (Table 3). The sensitivity model with constant trabecular elastic modulus, representing the upper bound (456 MPa) of the interquartile range, was significantly stiffer (lower strains) than the subject-specific model (Fig 9, middle panel) (Table 3). Although not statistically significant, models rep-

Table 2 Measurement of aluminum tube wall thickness from CT data. Errors in wall thickness were less than 10% for thicknesses greater than or equal to 0.762 mm. Errors increased progressively as the wall thickness decreased.

True thickness (mm)	Estimated thickness (mm) (mean±SD)	Error (%)
0.127	0.554±0.094	336
0.254	0.669±0.111	163
0.381	0.638±0.089	67
0.508	0.815±0.079	60
0.635	0.709±0.071	12
0.762	0.825±0.063	8.3
1.016	1.039±0.088	2.2
1.270	1.317±0.077	3.7
2.032	1.982±0.078	−2.5
2.921	2.781±0.108	−4.8

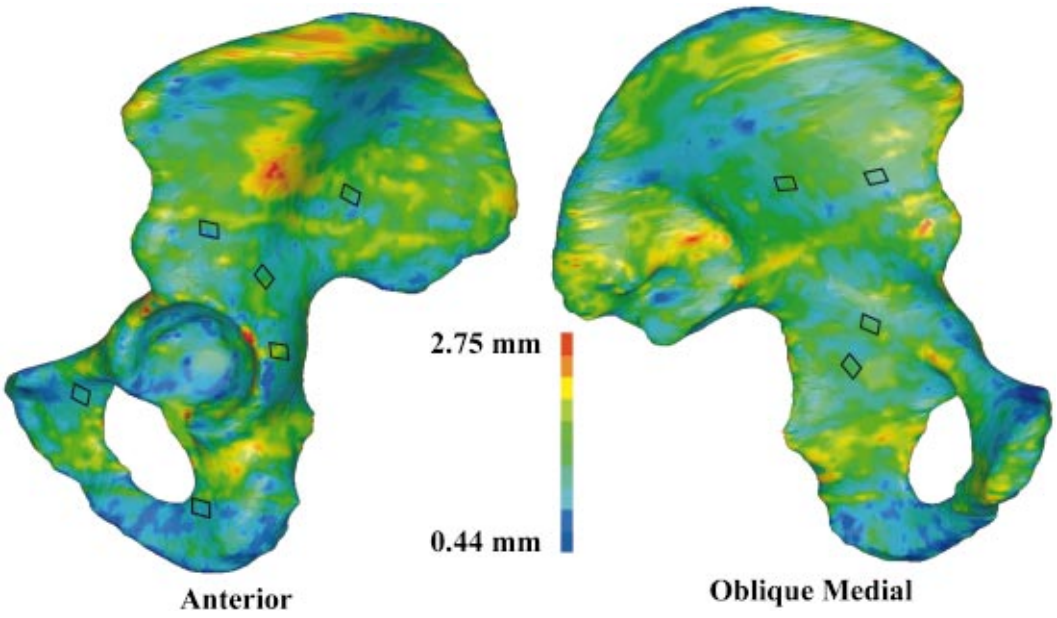

Fig. 7 Contours of position dependent cortical bone thickness with rectangles indicating the locations of the ten strain gauges used during experimental loading. Left panel—anterior view, right panel—medial view. Cortical thickness was highest along the iliac crest, the ascending pubis ramus, at the gluteal surface and around the acetabular rim. Areas of thin cortical bone were located at the acetabular cup, the ischial tuberosity, the iliac fossa, and the area surrounding the pubic tubercle. Cortical thickness beneath the surface of the strain gauges was similar to the average model thickness of 1.41 mm but deviated less.

resenting the median (164 MPa) and lower bound (45 MPa) of trabecular elastic modulus were also stiffer than the subject-specific model (Fig 9, middle panel), (Table 3).

Changes in the thickness of the cortical bone had a profound effect on cortical strains (Fig 9, bottom panel), for both ±0.5, 1 SD (Table 3). Using a ratio of average sensitivities, cortical surface strains were approximately ten times more sensitive to changes in cortical thickness than to alterations to trabecular bone elastic modulus (Table 3). The model with average cortical thickness predicted strains that were statistically similar to subject-specific model results (Table 3). FE predictions were significantly stiffer than the subject-specific model predictions when both average thickness and trabecular elastic modulus were used (Table 3). Changes to the cortical bone elastic modulus were significantly different than the subject-specific model for $E=15.38$ MPa but were not for $E=18.62$ MPa. However, values of the sensitivity parameter for the cortical bone modulus models were actually greater than those for changes to cortical thickness. This suggests that the pelvic FE model was very sensitive to changes in cortical bone modulus despite the fact that statistical significance was not obtained for both models. On average, FE predicted strains were

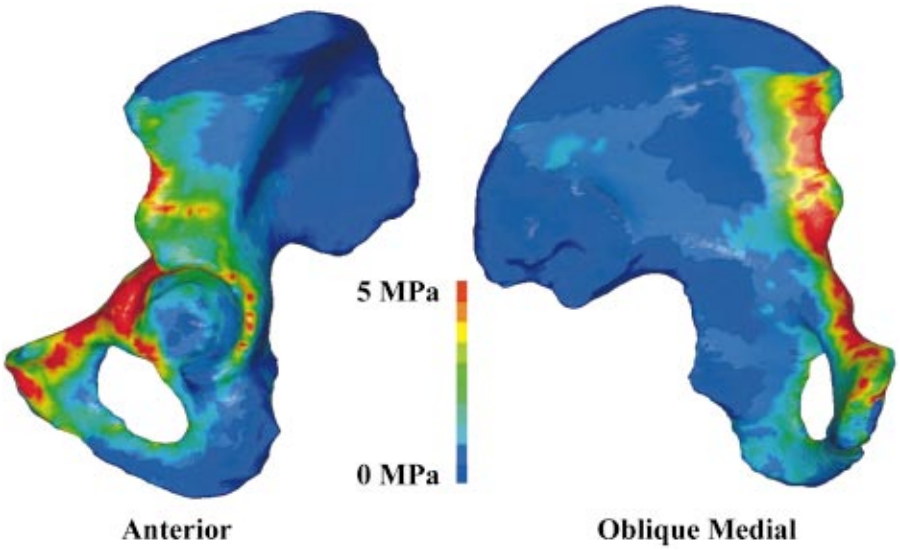

Fig. 8 Distribution of von Mises stress at 1 X body weight. Left panel—anterior view, right panel—medial view. Areas of greatest stress were near the pubis-symphasis joint, superior acetabular rim, and on the ilium just superior to the acetabulum.

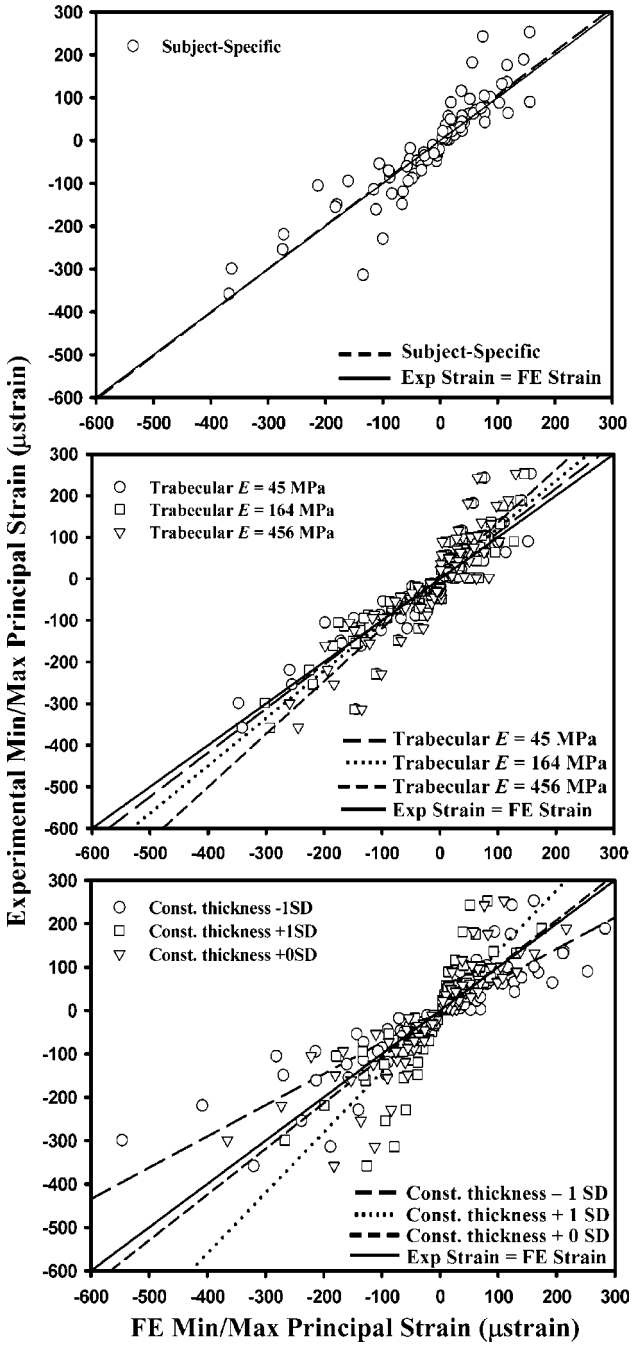

Fig. 9 FE predicted versus experimental cortical bone principal strains. Top panel—subject specific, middle panel—constant trabecular modulus, bottom panel—constant cortical thickness. For the subject-specific model there was strong correlation between FE predicted strains with those that were measured experimentally with a best-fit line that did not differ significantly from the line $y=x$ (experimental strains =FE predicted strains). Changes to the trabecular modulus did not have as significant of an effect on the resulting cortical bone strains as did changes to cortical bone thickness.

15 times more sensitive to alterations to the cortical bone elastic modulus than they were to changes in the trabecular bone elastic modulus. The remaining sensitivity models had best-fit lines that were not statistically different than the subject-specific model (Table 3). Sensitivity values for the remaining models were also comparable to those of the constant trabecular bone modulus, which suggests that FE predicted strains were not very sensitive to changes in cartilage modulus, cartilage thickness, cortical bone Poisson's ratio, and trabecular bone Poisson's ratio (Table 3). The best-fit line for the overlap sensitivity model was nearly identical to the subject-specific model, which suggests that FE predicted surface strains were not sensitive to overlap between the cortical shell and trabecular tetrahedral element.

Discussion

The most accurate FE model predictions were obtained when position-dependent cortical thickness and elastic modulus were used. When constant cortical bone thickness and trabecular bone elastic modulus were used, the model was significantly stiffer than the subject-specific model, so our second hypothesis was accepted. However, FE predictions of cortical strains were not statistically different than predictions from the subject-specific model when an average cortical thickness was used. Cortical shell thicknesses at the locations of the strains gauges were very close to the average thickness for the pelvis, but showed less deviation [1.38 ± 0.27 mm (SD)]. Since the sensitivity parameter showed that cortical bone strains were very sensitive to changes in cortical thickness (Table 3), this suggests that the similarity in results was most likely attributable to comparable thickness estimates (Fig. 7).

Cortical bone was represented using three-node shell elements. This choice was based on compatibility with the tetrahedral elements used for the trabecular bone and considerations of element accuracy. Tetrahedral elements were used for the trabecular bone because they allow automatic mesh generation based on Delaunay tesselation. Thick shells (wedges) and pentahedral (prismatic) solid elements were considered for the cortex but were later rejected since they produced inaccurate predictions of tip deflection when modeling cantilever beam bending.

Since the geometry of the model was based on the outer cortical surface, with a shell reference surface positioned to align with the top of the cortical surface, there was an overlap between the shell and tetrahedral solid elements. In theory, this overlap could produce inaccurate estimations of cortical surface strain. If this were the case then the sensitivity model that assigned the maximum trabecular elastic modulus to all surface tetrahedral nodes would have been stiffer than the subject-specific model. However, the results showed that this was not the case. To remove the overlap, a layer of thin shells could be placed at the interface between cortical and trabecular bone with thickness defined toward the outer cortex of the pelvis. However, this approach would not represent the surface topology of the pelvis as accurately as meshing the outer surface with tetrahedral elements. FE studies that aim to investigate the mechanics at the interface between cortical bone and trabecular bone should consider modeling the cortex without overlap.

Differences in boundary conditions, material properties, and applied loading make it impossible to compare FE predictions of stresses and strains in this study with previous investigations. The peak values of von Mises stress in this study appear to be unrealistic since bone would degenerate under such high, repetitive stresses [44]. However, high stresses were confined to a very small area that represented the location of contact between the head of the prosthetic femur and acetabulum and were still well below published values for ultimate stress [44].

It is likely that a more physiological loading condition would generate better femoral head coverage and thus reduce the peak stresses at the contact interface. On average, the von Mises stresses for cortical bone in the region of contact changed by 29% and 38% when cartilage thickness was reduced to 0 mm or increased to 4 mm, respectively. However, the slopes of the regression lines for these sensitivity models were very similar to the subject-specific model (Table 3). Although cortical surface strains were not sensitive to cartilage thickness, the local stresses and strains could be highly dependent on cartilage material properties and thickness. Nevertheless, the average stresses for areas of strain gauge attachment, away from the applied load, were very

Table 3 Results for all FE models including best-fit lines, r^2, values and sensitivity parameters. Best-fit lines were generated in reference to experimentally measured values of strain. Lines with slopes significantly different than the subject-subject model are indicated ($^{*}p<0.05$, $^{**}p<0.01$). All r^2 values were not significantly different than the subject-specific model. *Y* intercepts for all lines shown were not significantly different from zero. Higher values of sensitivity indicate a greater sensitivity to alterations in the model input/parameter.

Model type	Value	Best-fit line	r^2	Sensitivity
Subject-specific	NA	$y=1.015x+4.709$	0.824	NA
Const. cortical thick. (mm)	1.41	$y=1.054x-2.823$	0.754	NA
	1.66	$y=1.193x+2.265^{*}$	0.732	0.743
	1.17	$y=0.890x-2.820^{*}$	0.770	0.914
	1.90	$y=1.395x-2.059^{**}$	0.728	0.931
	0.92	$y=0.720x-2.248^{**}$	0.789	0.911
Const. trabecular *E* (MPa)	164	$y=1.142x+7.094$	0.833	NA
	45	$y=1.059x+5.371$	0.841	0.100
	456	$y=1.272x+8.370^{**}$	0.810	0.064
Const. thick. and *E* (mm, MPa)	1.41, 164	$y=1.204x+2.559^{*}$	0.767	NA
Cortical ν	$\nu=0.2$	$y=0.956x+9.460$	0.764	0.187
	$\nu=0.39$	$y=0.898x+3.294$	0.788	0.334
Trabecular ν	$\nu=0.29$	$y=1.013x+4.507$	0.824	0.005
Cortical *E* (GPa)	15.38	$y=0.840x+6.670^{**}$	0.777	1.82
	18.62	$y=1.107x+4.622$	0.821	0.951
Cartilage thick. (mm)	0.0	$y=0.952x+12.294$	0.780	0.062
	4.0	$y=1.072x+5.590$	0.841	0.056
Cartilage *E* (MPa)	1.36	$y=1.015x+4.711$	0.824	0.001
	7.79	$y=1.019x+4.715$	0.827	0.004
Overlap (MPa)	$E_{\text{suface nodes}}=3829$	$y=1.024x+5.119$	0.832	NA

similar to those reported by Dalstra et al. [26]. The value for peak von Mises stress was also consistent with Schuller and coworkers who conducted a FE investigation to model single-leg stance in which peak values of von Mises stresses were as high as 50 MPa [45].

Early models of the pelvis were either simplified 2D [46–48] or axisymmetric models [49,50]. Most three-dimensional FE models [26,45,51–56] used simplified pelvic geometry, average material properties, and/or did not validate FE predictions of stress and strain. The work of Dalstra et al. was the first and only attempt to develop and validate a three-dimensional FE model of the pelvis using subject-specific geometry and material properties [26]. The FE model was validated using experimental measures of strain in the periacetabular region of a cadaveric pelvis, but subject-specific experimental measurements were not performed. Different cadaveric specimens were used for FE mesh generation and experimental tests. In fact, it was reported that the acetabulum of the experimental test sample was 45 mm whereas that of the specimen used for FE geometry and material properties was 62 mm [26]. Subject-specific FE strains were compared to models that assumed constant cortical thickness and elastic modulus. FE model accuracy was more dependent on cortical bone thickness than trabecular elastic modulus, although statistical tests were not performed to support this conclusion. The effect of using average estimates was not investigated. Moreover, the effects of alterations in other bone and cartilage material properties were not investigated.

FE model predictions of cortical strain were relatively insensitive to most model inputs (except cortical thickness and modulus), but it is likely that FE strain predictions would change substantially if an idealized geometry was used rather than a faithful representation of the external geometry. Previously developed FE models of the pelvis have been based on coarse geometric representations. For example, Dalstra et al. hand-digitized 6 mm thick CT slices, which was ten times the thickness used in this study [26]. In this study, the small slice thickness and robust surface reconstruction techniques yielded a very accurate representation of the original geometry (Fig. 6). The present approach allowed cortical bone thickness to be estimated without laborious hand digitization [26]. While it may be acceptable to model the pelvis with idealized geometry for some applications, it is absolutely crucial to use accurate pelvic morphology if the research objective is to study diseases in which geometry is abnormal such as pelvic dysplasia.

The relative importance of model input parameters will depend heavily on the FE model predictions that are of interest. For this study deviations to the trabecular elastic modulus only had a significant effect on cortical surface strains when the upper interquartile range of trabecular bone elastic modulus was assessed. However, one should refrain from concluding that a position-dependent trabecular modulus is not important since it was shown that the model that assumed average cortical thickness and trabecular modulus was not as accurate as the baseline model. In addition, results for position-dependent thickness and constant trabecular modulus were stiffer than the subject-specific model, although the slopes were not significantly different over the entire interquartile range. Finally, FE predictions of overall model displacement were altered considerably when a constant trabecular modulus was used (data not shown). This change in model displacement did not result in significant deviations of strain for the cortex beneath the gauges but could have altered the surface strain at other locations. Therefore, it is recommended that a position-dependent trabecular bone modulus be included to improve overall FE model accuracy.

Although the results of the sensitivity studies suggest that changes in material properties (except for under/over-estimation of cortical bone elastic modulus) were not likely to produce significant changes in cortical bone surface strains, it is likely that strains would be more sensitive to changes in the boundary conditions and applied loading conditions. For this reason, it was not the intent of this proof of concept study to replicate physiological loading conditions. The use of a well-defined experimental loading configuration allowed accurate replication of the loading conditions in the FE model. Future studies will investigate pelvic mechanics under physiological loading conditions using additional experimental data.

A limitation to this study was the fact that the contralateral hemipelvis was not incorporated in the FE model. Nodes along the pubis joint were constrained, but some deflection may have occurred at the pubis joint in the experiment. If this were the case,

the strains near the pubis joint and along the ischium should have been much lower than other areas around the acetabular rim. However, strains were found to be greatest at the pubis joint and ischium during the experimental study, which was then confirmed by the FE results. If compression did occur at the pubis joint, it was probably minimal since deflection to this joint would act as an immediate strain relief to the pubis and ischium. Palpation of the pubic cartilage demonstrated that the joint appeared to be an extension of the trabecular bone, which suggests that the joint was relatively stiff.

CT is notorious for overestimating the thickness of cortical bone. Measurement accuracy depends largely on the axial and longitudinal resolution of the acquisition matrix and CT scanner collimation. The accuracy also depends on the energy settings, pitch, and reconstruction algorithm. Prevrhal et al. [37] determined that cortical bone thickness could be estimated within 10% for cortices that were equal to or greater than the minimum collimation of the CT scanner, which was approximately 0.7 mm for their scanner. Errors increased progressively for cortices that were less than the minimum collimation [37]. In the present study, a cortical bone phantom was used to assess the measurement limits of the CT scanner and segmentation procedure simultaneously. Results demonstrated that cortical thickness could be measured down to approximately 0.7 mm thick with less than 10% error.

In conclusion, our approach for subject-specific FE modeling of the pelvis has the ability to predict cortical bone strains accurately during acetabular loading. Cortical bone strains were most sensitive to changes in cortical thickness and cortical bone elastic modulus. Deviations in other assumed and estimated input parameters had little effect on the predicted cortical strains. Our approach has the potential for application to individual patients based on volumetric CT scans. This will provide a means to examine the biomechanics of the pelvis for cases when subject-specific geometry is important, such as in the case of pelvic dysplasia.

Acknowledgments

Financial support from the Orthopaedic Research and Education Foundation, University of Utah Seed Grant No. 2207083 and the Department of Orthopedics, University of Utah is gratefully acknowledged.

References

[1] Bergmann, G., Graichen, F., and Rohlmann, A., 1993, "Hip Joint Loading During Walking and Running, Measured in Two Patients," J. Biomech., **26**, pp. 969–990.
[2] Bergmann, G., Deuretzbacher, G., Heller, M., Graichen, F., Rohlmann, A., Strauss, J., and Duda, G. N., 2001, "Hip Contact Forces and Gait Patterns from Routine Activities," J. Biomech., **34**, pp. 859–871.
[3] Michaeli, D. A., Murphy, S. B., and Hipp, J. A., 1997, "Comparison of Predicted and Measured Contact Pressures in Normal and Dysplastic Hips," Med. Eng. Phys., **19**, pp. 180–186.
[4] Ochsner, M. G., Jr., Hoffman, A. P., DiPasquale, D., Cole, F. J., Jr., Rozycki, G. S., Webster, D. W., and Champion, H. R., 1992, "Associated Aortic Rupture-Pelvic Fracture: An Alert for Orthopedic and General Surgeons," J. Trauma, **33**, pp. 429–434.
[5] Rothenberger, D. A., Fischer, R. P., Strate, R. G., Velasco, R., and Perry, J. F., Jr., 1978, "The Mortality Associated with Pelvic Fractures," Surgery, **84**, pp. 356–361.
[6] Adams, P., Davies, G. T., and Sweetnam, P., 1971, "Cortical Bone-Loss with Age," Lancet, **2**, pp. 1201–1202.
[7] Bombelli, R., 1983, *Osteoarthritis of the Hip*, Springer-Verlag, Berlin, Germany.
[8] Croft, P., Cooper, C., Wickham, C., and Coggon, D., 1991, "Osteoarthritis of the Hip and Acetabular Dysplasia," Ann. Rheum. Dis., **50**, pp. 308–310.
[9] Parfitt, A. M., 1984, "Age-Related Structural Changes in Trabecular and Cortical Bone: Cellular Mechanisms and Biomechanical Consequences," Calcif. Tissue Int., **36**, pp. S123–S128.
[10] Solomon, L., 1976, "Patterns of Osteoarthritis of the Hip," J. Bone Joint Surg. Br., **58**, pp. 176–183.
[11] Stulberg, S. D., and Harris, W. H., 1974, "Acetabular Dysplasia and Development of Osteoarthritis of the Hip," *Proceedings of the Second Open Scientific Meeting of the Hip Society*, pp. 82–93.
[12] Harris, W. H., 1986, "Etiology of Osteoarthritis of the Hip," Clin. Orthop., pp. 20–33.
[13] Murray, R. O., 1965, "The Aetiology of Primary Osteoarthritis of the Hip," Br. J. Radiol., **38**, pp. 810–824.
[14] Afoke, N. Y., Byers, P. D., and Hutton, W. C., 1987, "Contact Pressures in the Human Hip Joint," J. Bone Joint Surg. Br., **69**, pp. 536–541.
[15] Brown, T. D. and Shaw, D. T., 1983, "In Vitro Contact Stress Distributions in the Natural Human Hip," J. Biomech., **16**, pp. 373–384.
[16] Day, W. H., Swanson, S. A., and Freeman, M. A., 1975, "Contact Pressures in the Loaded Human Cadaver Hip," J. Bone Joint Surg. Br., **57**, pp. 302–313.
[17] Hodge, W. A., Fijan, R. S., Carlson, K. L., Burgess, R. G., Harris, W. H., and Mann, R. W., 1986, "Contact Pressures in the Human Hip Joint Measured in Vivo," Proc. Natl. Acad. Sci. U.S.A., **83**, pp. 2879–2883.
[18] Ipavec, M., Brand, R. A., Pedersen, D. R., Mavcic, B., Kralj-Iglic, V., and Iglic, A., 1999, "Mathematical Modeling of Stress in the Hip During Gait," J. Biomech., **32**, pp. 1229–1235.
[19] Ipavec, M., Iglic, A., Iglic, V. K., and Srakar, F., 1996, "Stress Distribution on the Hip Joint Articular Surface During Gait," Pfluegers Arch., **431**, pp. R275–R276.
[20] Mavcic, B., Antolic, V., Brand, R., Iglic, A., Kralj-Iglic, V., and Pedersen, D. R., 2000, "Peak Contact Stress in Human Hip During Gait," Pfluegers Arch., **440**, pp. R177–R178.
[21] Mavcic, B., Pompe, B., Antolic, V., Daniel, M., Iglic, A., and Kralj-Iglic, V., 2002, "Mathematical Estimation of Stress Distribution in Normal and Dysplastic Hips," J. Orthop. Res., **20**, pp. 1025–1030.
[22] Calvo, E., Palacios, I., Delgado, E., Ruiz-Cabello, J., Hernandez, P., Sanchez-Pernaute, O., Egido, J., and Herrero-Beaumont, G., 2001, "High-Resolution MRI Detects Cartilage Swelling at the Early Stages of Experimental Osteoarthritis," Osteoarthritis Cartilage, **9**, pp. 463–472.
[23] Gupta, K. B., Duryea, J., and Weissman, B. N., 2004, "Radiographic Evaluation of Osteoarthritis," Radiol. Clin. North Am., **42**, pp. 11–41, v.
[24] Fazzalari, N. L., Moore, R. J., Manthey, B. A., and Vernon-Roberts, B., 1992, "Comparative Study of Iliac Crest and Subchondral Femoral Bone in Osteoarthritic Patients," Bone (N.Y.) **13**, pp. 331–335.
[25] Fischer, K. J., Manson, T. T., Pfaeffle, H. J., Tomaino, M. M., and Woo, S. L., 2001, "A Method for Measuring Joint Kinematics Designed for Accurate Registration of Kinematic Data to Models Constructed from CT Data," J. Biomech., **34**, pp. 377–383.
[26] Dalstra, M., Huiskes, R., and van Erning, L., 1995, "Development and Validation of a Three-Dimensional Finite Element Model of the Pelvic Bone," ASME J. Biomech. Eng., **117**, pp. 272–278.
[27] Pytel, A. and Kiusalaas, J., 2003, *Mechanics of Materials*, vol. 14. Thomson, Pacific Grove, CA.
[28] Boissonnat, J.-D., 1988, "Shape Reconstruction from Planar Cross-Sections," Comput. Vis. Graph. Image Process., **44**, pp. 1–29.
[29] Schroeder, W. J., Zarge, J., and Lorenson, W. E., 1992, "Decimation of Triangle Meshes,"ACM SIGGRAPH Computer Graphics, **26**, pp. 65–70.
[30] Taubin, G., Zhang, T., and Golub, G., 1996. "Optimal Surface Smoothing as Filter Design," Stanford University IBM RC-20404.
[31] Schroeder, W. J., Avila, L. S., and Hoffman, W., 2002, *The Visualization Toolkit: An Object Oriented Approach to Computer Graphics*, 3rd ed. Kitware Inc., Clifton Park, NY.
[32] Pawlak, T. P., and Yunus, S. M., 1991, "Solid Elements with Rotational Degrees of Freedom: Part II. Tetrahedron Elements," Int. J. Numer. Methods Eng., **31**, pp. 593–610.
[33] Ahmad, S., 1970, "Analysis of Thick and Thin Shell Structures," Int. J. Numer. Methods Eng., **2**, pp. 419–451.
[34] Hughes, T. J. R., and Liu, W. K., 1981, "Nonlinear Finite Element Analysis of Shells: Part I. Two Dimensional Shells.," Comput. Methods Appl. Mech. Eng., **27**, pp. 167–181.
[35] Hughes, T. J. R. and Liu, W. K., 1981, "Nonlinear Finite Element Analysis of Shells: Part II. Three Dimensional Shells.," Comput. Methods Appl. Mech. Eng., **27**, pp. 331–362.
[36] Hughes, T. J., 1980, "Generalization of Selective Integration Procedures to Anisotropic and Nonlinear Media," Int. J. Numer. Methods Eng., **15**, pp. 1413–1418.
[37] Prevrhal, S., Engelke, K., and Kalender, W. A., 1999, "Accuracy Limits for the Determination of Cortical Width and Density: The Influence of Object Size and CT Imaging Parameters," Phys. Med. Biol., **44**, pp. 751–764.
[38] Nickoloff, E. L., Dutta, A. K., and Lu, Z. F., 2003, "Influence of Phantom Diameter, Kvp and Scan Mode Upon Computed Tomography Dose Index," Med. Phys., **30**, pp. 395–402.
[39] Suzuki, S., Yamamuro, T., Okumura, H., and Yamamoto, I., 1991, "Quantitative Computed Tomography: Comparative Study Using Different Scanners with Two Calibration Phantoms," Br. J. Radiol., **64**, pp. 1001–1006.
[40] Dalstra, M., Huiskes, R., Odgaard, A., and van Erning, L., 1993, "Mechanical and Textural Properties of Pelvic Trabecular Bone," J. Biomech., **26**, pp. 523–535.
[41] Mooney, M., 1940, "A Theory of Large Elastic Deformation," J. Appl. Phys., **11**, pp. 582–592.
[42] Little, R. B., Wevers, H. W., Siu, D., and Cooke, T. D., 1986, "A Three-Dimensional Finite Element Analysis of the Upper Tibia," ASME J. Biomech. Eng., **108**, pp. 111–119.
[43] Cohen, J., Cohen, P., West, S. G., and Aiken, L. S., 2003, *Applied Multiple Regression Analysis for the Behavioral Sciences*, 3rd ed. Lawrence Erlhaum Associates, Mahwah, NJ.
[44] Evans, F. G., 1973, *Mechanical Properties of Bone*. Thomas, Springfield, IL.
[45] Schuller, H. M., Dalstra, M., Huiskes, R., and Marti, R. K., 1993, "Total Hip Reconstruction in Acetabular Dysplasia. A Finite Element Study," J. Bone

Joint Surg. Br., **75**, pp. 468–474.
[46] Vasu, R., Carter, D. R., and Harris, W. H., 1982, "Stress Distributions in the Acetabular Region--I. Before and after Total Joint Replacement," J. Biomech., **15**, pp. 155–164.
[47] Carter, D. R., Vasu, R., and Harris, W. H., 1982, "Stress Distributions in the Acetabular Region--II. Effects of Cement Thickness and Metal Backing of the Total Hip Acetabular Component," J. Biomech., **15**, pp. 165–170.
[48] Rapperport, D. J., Carter, D. R., and Schurman, D. J., 1985, "Contact Finite Element Stress Analysis of the Hip Joint," J. Orthop. Res., **3**, pp. 435–446.
[49] Pedersen, D. R., Crowninshield, R. D., Brand, R. A., and Johnston, R. C., 1982, "An Axisymmetric Model of Acetabular Components in Total Hip Arthroplasty," J. Biomech., **15**, pp. 305–315.
[50] Huiskes, R., 1987, "Finite Element Analysis of Acetabular Reconstruction. Noncemented Threaded Cups," Acta Orthop. Scand., **58**, pp. 620–625.
[51] Dalstra, M. and Huiskes, R., 1995, "Load Transfer across the Pelvic Bone," J. Biomech., **28**, pp. 715–724.
[52] Spears, I. R., Pfleiderer, M., Schneider, E., Hille, E., and Morlock, M. M., 2001, "The Effect of Interfacial Parameters on Cup-Bone Relative Micromotions. A Finite Element Investigation," J. Biomech., **34**, pp. 113–120.
[53] Garcia, J. M., Doblare, M., Seral, B., Seral, F., Palanca, D., and Gracia, L., 2000, "Three-Dimensional Finite Element Analysis of Several Internal and External Pelvis Fixations," ASME J. Biomech. Eng., **122**, pp. 516–522.
[54] Konosu, A., 2003, "Development of a Biofidelic Human Pelvic Fe-Model with Several Modifications onto a Commercial Use Model for Lateral Loading Conditions," proceedings of the *SAE International*, pp. 85–100.
[55] Oonishi, H., Isha, H., and Hasegawa, T., 1983, "Mechanical Analysis of the Human Pelvis and Its Application to the Artificial Hip Joint--by Means of the Three Dimensional Finite Element Method," J. Biomech., **16**, pp. 427–444.
[56] Dawson, J. M., Khmelniker, B. V., and McAndrew, M. P., 1999, "Analysis of the Structural Behavior of the Pelvis During Lateral Impact Using the Finite Element Method," Accid. Anal Prev., **31**, pp. 109–119.
[57] Lappi, V. G., King, M. S., and Lemay, I., 1979, "Determination of Elastic Constants for Human Femurs," ASME J. Biomech. Eng., **101**, pp. 193–197.
[58] Snyder, S. M. and Schneider, E., 1991, "Estimation of Mechanical Properties of Cortical Bone by Computed Tomography," J. Orthop. Res., **9**, pp. 422–431.
[59] Armstrong, C. G., Bahrani, A. S., and Gardner, D. L., 1979, "In Vitro Measurement of Articular Cartilage Deformations in the Intact Human Hip Joint under Load," J. Bone Joint Surg. Br., **61**, pp. 744–755.